

# Properties of Ion-Implanted Junctions in Mercury-Cadmium-Telluride

A. KOLODNY AND I. KIDRON, MEMBER, IEEE

**Abstract**—The formation of n-p junctions by ion-implantation in  $\text{Hg}_{0.71}\text{Cd}_{0.29}\text{Te}$  is shown to be a result of implantation damage. n-p photodiodes have been made by implantation of Ar, B, Al, and P in a p-type substrate with acceptor concentration of  $4 \times 10^{16} \text{ cm}^{-3}$ . The implanted n-type layer is characterized by sheet electron concentration of  $10^{14}$  to  $10^{15} \text{ cm}^{-2}$  and electron mobility higher than  $10^3 \text{ cm}^2 \cdot \text{V}^{-1} \cdot \text{s}^{-1}$ , for ion doses in the range  $10^{13}$ – $5 \times 10^{14} \text{ cm}^{-2}$ . The photodiodes have a spectral cutoff of  $5.2 \mu\text{m}$ , quantum efficiency higher than 80 percent, and differential resistance by area product above  $2000 \Omega \cdot \text{cm}^2$  at 77 K. The temperature dependence of the differential resistance is discussed. The junction capacitance dependence on reverse voltage fits a linearly graded junction model. Reverse current characteristics at 77 K have been investigated using gate-controlled diodes. The results suggest that reverse breakdown is dominated by interband tunneling in field-induced junctions at the surface, for both polarities of surface potential.

## I. INTRODUCTION

THE TECHNIQUE of ion implantation has a special advantage over methods based on diffusion for fabrication of p-n junctions in  $\text{Hg}_{1-x}\text{Cd}_x\text{Te}$ , since it permits precise control of junction depth, allows usage of various dopants, and avoids heating of this metallurgically sensitive material. Ion-implanted photodiodes have been reported by several authors [1]–[8]. In all of the reported devices n-type layers were formed on p-type substrates by implantation of Hg [3], [4], In [2], Al [1], B [6], [7], or bombardment by protons [8]. Some authors mention that post-implant annealing at room temperature was sufficient for junction formation [3]–[5]. Often n-p junctions in HgCdTe are characterized by soft breakdown at relatively low reverse bias. In addition, their differential resistance by area product is, in many cases, limited by shunt conductance attributed to surface leakage.

This work reports further experimental results on implanted n-p junctions in  $\text{Hg}_{0.71}\text{Cd}_{0.29}\text{Te}$ . Our results indicate that implantation damage is the primary cause for conversion of p-type HgCdTe to n type. In fact, we have obtained essentially the same results by implantation of boron and aluminum (which are known to be donors [9]), argon (which is chemically neutral), and phosphorus (known as an acceptor [9]). An account of the implantation effects is given in the following section. Electrical and electrooptical properties of the devices are described in subsequent sections. The temperature dependence of the differential resistance by area product, which is the key parameter for photovoltaic detector per-

TABLE I  
PROPERTIES OF ION-IMPLANTED LAYERS IN p-TYPE  $\text{Hg}_{0.71}\text{Cd}_{0.29}\text{Te}$  AFTER ANNEALING FOR 12 h AT  $65^\circ\text{C}$

Implanted Ion	Energy (keV)	Dose ( $\text{cm}^{-2}$ )	Number of carriers per unit area in the implanted layer ( $\text{cm}^{-2}$ )	Effective carrier mobility in the implanted layer ( $\text{cm}^2 \cdot \text{Volt}^{-1} \cdot \text{sec}^{-1}$ )
B <sup>+</sup>	100	$10^{13}$	n-type, $5 \times 10^{14}$	2900
B <sup>+</sup>	100	$10^{14}$	n-type, $6 \times 10^{14}$	1700
B <sup>+</sup>	100	$5 \times 10^{14}$	n-type, $6.25 \times 10^{14}$	1230
P <sup>+</sup>	300	$10^{14}$	n-type, $6.25 \times 10^{14}$	940
Ar <sup>+</sup>	300	$10^{14}$	n-type, $6 \times 10^{14}$	1000

formance, is studied. At temperatures above 150 K the  $R_0A$  product is governed by carrier diffusion from the p-type bulk, and is limited by low minority carrier lifetime. Between 150 and 115 K, the limiting mechanism is generation-recombination in the junction depletion region. Below 115 K, the  $R_0A$  product is dominated by surface leakage currents. The origin of reverse breakdown and leakage current has been investigated using a gate-controlled junction device. From the device characteristics we conclude that leakage and breakdown are probably caused by tunneling of carriers to field-induced junctions near the surface.

## II. EFFECTS OF ION IMPLANTATION ON p-TYPE HgCdTe

The starting material in our experiments was p-type  $\text{Hg}_{0.71}\text{Cd}_{0.29}\text{Te}$  grown by the method of solid-state recrystallization [21]. Wafers of random orientation were annealed at approximately  $350^\circ\text{C}$  [22] to obtain carrier concentration in the range  $1$ – $5 \times 10^{16} \text{ cm}^{-3}$ , caused by native defects, and Hall mobility of  $250 \text{ cm}^2 \cdot \text{V}^{-1} \cdot \text{s}^{-1}$  at 77 K. Implantation of B, Al, P, and Ar was performed at room temperature with doses of  $10^{13}$ – $10^{15} \text{ cm}^{-2}$  and energies of 100–300 keV. An n-type layer was formed on the surface by all the implantations attempted, as was evident from van der Pauw, photovoltaic effect and hot probe measurements at 77 K. The layer remained n type after annealing in vacuum at temperatures as high as  $140^\circ\text{C}$ . Results of several implantations are summarized in Table I.

The ion energies in Table I were selected in order to obtain approximately the same range in all cases. Ion energy was varied in implantation experiments performed at this laboratory on n-type  $\text{Hg}_{0.8}\text{Cd}_{0.2}\text{Te}$  [12], and was found to have only a small effect on the properties of the implanted layer.

The junction depth was typically less than  $1 \mu\text{m}$ , based on

Manuscript received April 12, 1979; revised September 11, 1979.  
The authors are with the Department of Electrical Engineering, Technion—Israel Institute of Technology, Haifa, Israel.

mesa etching measurements. This is in agreement with calculated values [10] (e.g., 100-keV  $B^+$  ions have a mean range of  $0.23 \mu\text{m}$  and straggle of  $0.14 \mu\text{m}$  in  $\text{Hg}_{0.71}\text{Cd}_{0.29}\text{Te}$ ).

The mobility and number of electrons in the implanted layer were measured by the van der Pauw method. The measured quantities are

$$\left(\frac{\bar{R}_H}{x_j}\right) = \frac{1}{q} \frac{\int_0^{x_j} \mu^2(x) n(x) dx}{\left[\int_0^{x_j} \mu(x) n(x) dx\right]^2} \quad (1)$$

$$(\bar{\sigma} \cdot x_j) = q \int_0^{x_j} \mu(x) n(x) dx \quad (2)$$

where  $\bar{R}_H$  and  $\bar{\sigma}$  denote average Hall coefficient and specific conductivity,  $\mu(x)$  and  $n(x)$  are mobility and carrier concentration at depth  $x$ , and  $x_j$  is the junction depth. Assuming a constant effective mobility throughout the implanted layer, the number of carriers in the layer is  $[q(\bar{R}_H/x_j)]^{-1}$ , and the effective mobility is  $[(\bar{R}_H/x_j) \cdot (\bar{\sigma} \cdot x_j)]$ . Measured values of mobility were typically in the range  $1000\text{--}2000 \text{ cm}^2 \cdot \text{V}^{-1} \cdot \text{s}^{-1}$ . The number of electrons in the implanted layer was  $10^{14}$  to  $10^{15} \text{ cm}^{-2}$ , almost independent of the implanted ion dose. For small ion doses, the number of electrons in the layer exceeded the number of implanted ions by an order of magnitude. The effective concentration of donors near the surface, as determined from  $C$ - $V$  characteristics of MOS capacitors (deposited on the surface with anodic oxide as insulator [11]) was found to be  $1\text{--}3 \times 10^{18} \text{ cm}^{-3}$ .

We conclude that n-type conductivity stems from ion implantation damage. This is based on the following observations:

- 1) The implanted layer parameters are not sensitive to the implanted ion identity and dose.
- 2) The number of carriers in the layer exceeds the number of implanted ions.
- 3) The layer is converted to n type without thermal annealing.

Other authors [3]–[5] have observed the lack of sensitivity of the layer properties to implantation parameters. The very small ion doses ( $10^{12}\text{--}10^{13} \text{ cm}^{-2}$ ) used by some authors [4], [5] to fabricate  $n^+$ -p junctions also support our results. The same conclusion has been reached concurrently at this laboratory [12] in implantation experiments on n-type  $\text{Hg}_{0.8}\text{Cd}_{0.2}\text{Te}$ .

Thermal treatment at  $60\text{--}80^\circ\text{C}$  caused a slight increase in the layer carrier concentration and mobility. The implantation effects were not annealed out in vacuum at temperatures as high as  $140^\circ\text{C}$ . Normally, HgCdTe devices are not heated above  $100^\circ\text{C}$  during processing.

### III. JUNCTION PROPERTIES

Both planar and mesa structure n-p photodiodes have been studied. Mesa devices were made by implanting on a bare surface and then using chemical etching for element separation. Evaporated ZnS was used as an insulating passivation layer and antireflection coating. Contacts to the implanted

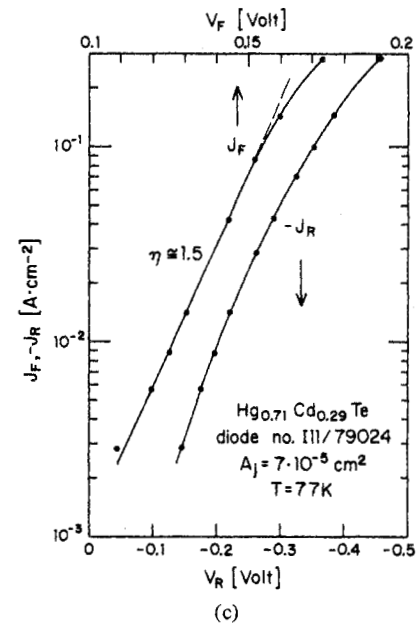
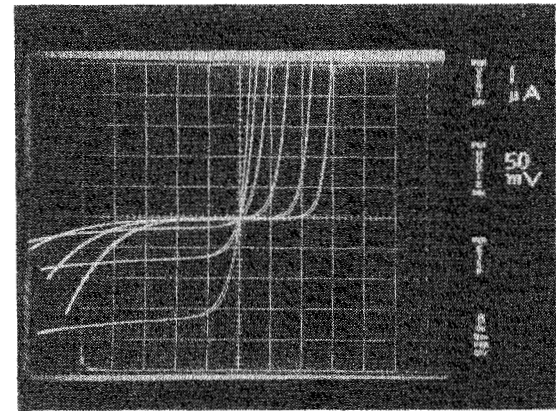
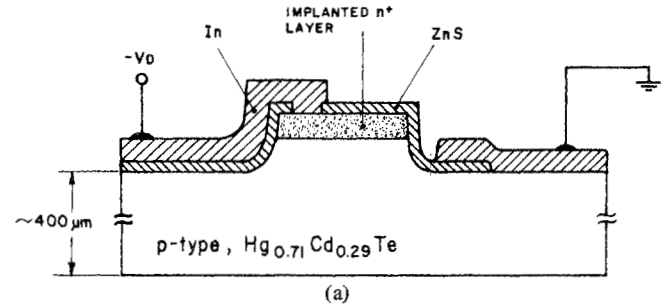


Fig. 1. (a) Cross-sectional diagram of the implanted diode. (b) Current-voltage characteristics of argon-implanted  $\text{Hg}_{0.71}\text{Cd}_{0.29}\text{Te}$  n-p diode at 84, 121, 160, 189, 208, and 219 K. The implanted dose is  $10^{15} \text{ cm}^{-2}$  with energy of 300 keV, into a substrate with  $4 \times 10^{16} \text{ cm}^{-3}$  acceptors. The junction area is  $7 \times 10^{-5} \text{ cm}^2$ . (c) Forward and reverse current-voltage characteristics of the same device, without background photon flux.

devices were made by etching windows in the ZnS and evaporating indium. Planar devices were made by performing the implantation through openings in thick photoresist. A cross-sectional diagram of the device is shown in Fig. 1(a).

Fig. 1(b) shows typical current-voltage characteristics of a diode made by argon implantation, at several temperatures in

the range 84–219 K. Very similar results were obtained by implantation of other species. Forward and reverse characteristics of this diode at 77 K are plotted in Fig. 1(c) on a semilogarithmic scale. The forward characteristics fit an exponential dependence of the form  $I_F = I_0 \exp(qV_F/\eta kT)$  with  $\eta \approx 1.5$ . The deviation from the straight line is due to a series resistance of about 500  $\Omega$ , so there may be a sizeable error in  $\eta$ . The series resistance is caused by the indium contact to the substrate. Reverse characteristics of the diode exhibit soft breakdown at relatively low voltages. It is difficult to define a breakdown voltage because the reverse current is increasing continuously, as may be seen in Fig. 1(b). By illuminating the diode, the reverse current increases by a constant amount irrespective of the reverse bias. If the “breakdown” were due to avalanche multiplication in the whole junction area, an amplification of the photocurrent at high reverse bias would be expected. In addition, the smooth continuous dependence of the reverse current on reverse voltage is not typical of an avalanche process. These observations, together with results on gate-controlled devices described below, indicate that tunneling near the surface at the circumference of the junction is very likely the cause of reverse current breakdown.

Measured junction capacitance at 1 MHz was measured at 77 K with a Boonton 71A and was found to fit a linearly graded junction better than an abrupt junction model, as can be seen from the slopes and intercepts in Fig. 2. Also, the zero-bias capacitance of  $6 \times 10^{-8} \text{ F} \cdot \text{cm}^{-2}$  was lower by a factor of 3 than the value calculated from substrate doping assuming an abrupt one-sided junction.

Differential resistance at zero bias, which effects photodiode noise, was measured versus temperature on a diode identical to the one of Fig. 1, but covered by metallization to prevent photon-induced currents. Fig. 3 shows the differential resistance by area product versus reciprocal temperature. Also shown are the theoretical curves according to a diffusion model and a depletion-region generation-recombination model.

#### Diffusion Model

In the diffusion model, we assume that the current density obeys the ideal diode relation

$$J = J_0 \exp(qV/kT) \quad (3)$$

so that the  $R_0A$  product is

$$(R_0A)_{\text{diff}} = \left. \frac{\partial V}{\partial J} \right|_{V=0} = \frac{kT}{qJ_0} \quad (4)$$

$J_0$  is the sum of diffusion current densities of minority carriers from both sides of the junction. The contribution of minority holes from the implanted layer to  $J_0$  is, assuming a step junction

$$J_{0p} = qD_p \cdot \frac{n_i^2}{N_D} \cdot \frac{1}{L_p \cdot \tanh(x_j/L_p)} \quad (5)$$

where  $D_p$  is the diffusion constant for holes,  $n_i$  the intrinsic carrier concentration,  $N_D$  the donor concentration,  $x_j$  is the

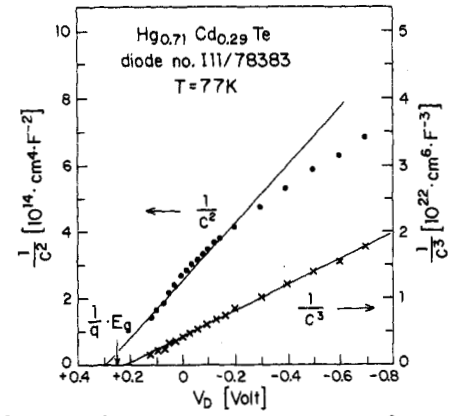


Fig. 2.  $1/C^2$  and  $1/C^3$  data versus reverse bias.  $1/C^3$  gives a reasonable intercept voltage below the bandgap. Junction area is  $5.7 \times 10^{-4} \text{ cm}^2$ , implanted with boron,  $5 \times 10^{14} \text{ cm}^{-2}$ , 150 keV.

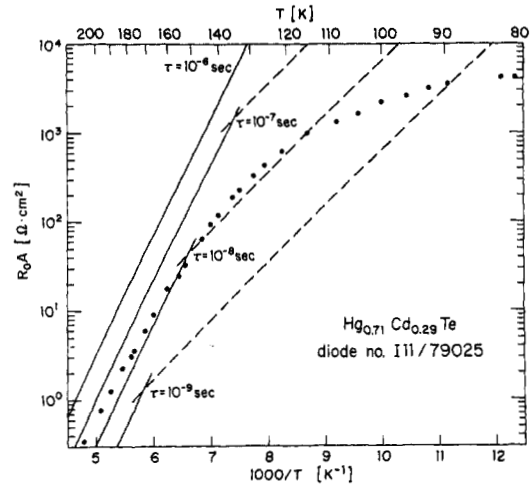


Fig. 3.  $R_0A$  product as a function of temperature for an argon-implanted diode with zero background. Also shown are theoretical values for a diffusion model (continuous lines) and generation-recombination model (dashed lines), for a few values of minority-carrier lifetime.

junction depth, and  $L_p$  is the diffusion length.  $L_p$  depends on the holes lifetime, which is expected to be dominated by Auger recombination. By evaluating (5) at 200 K, using  $N_D = 10^{18} \text{ cm}^{-3}$  (the calculated Auger lifetime [23] is in the order of  $10^{-10} \text{ s}$ ), and assuming  $D_p = 2.6 \text{ cm}^2 \cdot \text{s}^{-1}$  we can see that  $J_{0p}$  alone would lead to  $R_0A$  of about  $5 \Omega \cdot \text{cm}^2$ , which is higher than the measured value. Hence we assume that the contribution of the n side to  $J_0$  is not a limiting factor. The contribution of minority electrons from the crystal bulk is

$$J_{0n} = qD_n \frac{n_i^2}{N_A L_n} = q \frac{n_i^2}{N_A} \left( \frac{D_n}{\tau_n} \right)^{1/2} \quad (6)$$

where  $L_n = (D_n \cdot \tau_n)^{1/2}$  is the diffusion length for electrons. The corresponding  $R_0A$  product is

$$(R_0A)_{\text{diff}} = \frac{kT}{q^2} \frac{N_A}{n_i^2} \left( \frac{\tau_n}{D_n} \right)^{1/2} = \frac{1}{q} \frac{N_A}{n_i^2} \left( \frac{kT}{q} \frac{\tau_n}{\mu_n} \right)^{1/2} \quad (7)$$

The dominant temperature-dependent parameter in this expression is  $n_i^2$ . Equation (7) is plotted in Fig. 3 (continuous lines) for various values of the electron lifetime  $\tau_n$ , using

$N_A = 4 \times 10^{16} \text{ cm}^{-3}$ ,  $\mu_n = 2 \times 10^4 \text{ cm}^2 \cdot \text{V}^{-1} \cdot \text{s}^{-1}$ , and assuming that all the parameters except  $n_i$  are temperature independent. A recent expression [13] for  $n_i(T)$  has been used in the calculation

$$n_i(x, T) = \frac{1.265 \times 10^{16} T^{3/2} (6+x)^{-3/2} E_G^{3/2}}{1 + [1 + 19.4(6+x)^{-3/2} (m_n^*/m_0)^{-3/2} E_G^{3/2} \exp(E_G/kT)]^{1/2}} \text{ (cm}^{-3}\text{)} \quad (8)$$

where

$$E_G(x, T) = 6.006 \times 10^{-4} T(1 - 1.89x) + 1.948x - 0.337 \text{ (eV)}. \quad (9)$$

In comparison with an earlier expression given by Schmit [24], (8) yields  $n_i$  values which are smaller by a factor of about 1.5 for  $x = 0.29$ . However, this expression was preferred since it is based directly on Hall measurements performed on n-type samples of this composition. The best fit was obtained for  $m_n^*/m_0 = 0.9$  [13].

#### Depletion-Region Generation-Recombination Model

The  $R_0A$  product due to generation-recombination (g-r) in the depletion region via Shockley-Read-Hall centers located near midgap is [14]

$$(R_0A)_{\text{g-r}} = \frac{V_{bi}\tau_0}{qn_iW} \quad (10)$$

where  $\tau_0$  is an average carrier lifetime,  $V_{bi}$  is the built-in potential, and  $W$  is the depletion-region width. The value of  $V_{bi}/W$  changes only by a factor of about two over the whole temperature range of interest, so that  $V_{bi}$  and  $W$  may be calculated from  $C$ - $V$  measurements at 77 K without introducing a significant error. Resultant values are plotted in Fig. 3 (dashed lines) for several values of  $\tau_0$ . A continuous transition from the diffusion model to the g-r model is indicated, assuming that  $\tau_0$  coincides with the bulk lifetime  $\tau_n$ . The dominant process at each temperature is the one which gives the lower  $R_0A$  product.

A comparison of the experimental data with theoretical curves in Fig. 3 shows that at elevated temperatures the  $R_0A$  product of our devices follows the slope predicted by the diffusion model, i.e., varies with temperature as  $n_i^{-2}$ , which is approximately proportional to  $\exp(E_G/kT)$ . At intermediate temperatures, the  $R_0A$  product follows a slope corresponding to  $n_i^{-1}$ , as in the g-r model. At low temperatures, the theory predicts higher values than those observed experimentally, and this is probably due to leakage currents, discussed in the next section. We may conclude that our devices are diffusion limited above 150 K and generation-recombination limited between 150 and 115 K. The measured  $R_0A$  values correspond to a relatively low bulk lifetime of about  $10^{-8}$  s. Measurements of effective lifetime in p-type samples (based on photoconductivity experiments between 77 and 250 K) give results in the range  $5$ - $20 \times 10^{-9}$  s which is in general agreement with lifetime as deduced from diodes made on similar substrates.

For background-limited performance of a photodiode at a given temperature, its  $R_0A$  product should satisfy

$$\frac{4kT}{R_0A} \ll 2qJ_B = 2q^2\eta\phi_B \quad (11)$$

where  $\phi_B$  is the background photon flux per unit area,  $\eta$  is the

quantum efficiency, and  $J_B$  is the background-induced short-circuit current density. For prescribed cutoff wavelength and operating temperature, the molar fraction  $x$  of the material and the minority-carrier lifetime required to achieve such performance may be calculated from (7)-(11). An  $R_0A$  product above  $15 \Omega \cdot \text{cm}^2$  at 200 K detector temperature is desired for background-limited detection at  $5 \mu\text{m}$ , with  $180^\circ$  field of view at 300 K. The bulk lifetime of an n<sup>+</sup>-p photodiode should exceed  $10^{-5}$  s to achieve this. Such electron lifetimes have not been reported for p-type  $\text{Hg}_{1-x}\text{Cd}_x\text{Te}$  [6], [15]. Current n-type  $\text{Hg}_{0.71}\text{Cd}_{0.29}\text{Te}$  with electron concentration of about  $5 \times 10^{14} \text{ cm}^{-3}$  exhibits hole lifetime of the order of  $10^{-5}$  s in the temperature range 77-220 K [23], [25], in consistency with Auger recombination theory [23]. This suggests that a p<sup>+</sup>-on-n-type bulk diode could yield the afore-mentioned required  $R_0A$  product for background-limited operation.

#### IV. ELECTROOPTIC PROPERTIES

The relative spectral sensitivity, as measured on a typical diode, is shown in Fig. 4 in relative units per watt of incident radiation. The measurement was performed at a reverse bias of 75 mV, using a transimpedance amplifier. The photocurrent is divided between the differential resistance of the junction and the parasitic series resistance, so that with zero bias at elevated temperatures the quantum efficiency apparently decreases as the differential resistance becomes smaller. Measurement of responsivity at reverse bias, so that the differential resistance is relatively high, indicates that the quantum efficiency slowly increases with temperature almost up to 300 K. This behavior is believed to be a result of an increase in diffusion length for electrons in the p-type substrate, mainly due to an increase in electron lifetime. Such a dependence of lifetime on temperature was found in our photoconductivity experiments on p-type samples. Similar results were reported also from switching experiments on Schottky-barrier diodes made on p-type  $\text{HgCdTe}$  [26], and attributed to Shockley-Read-Hall recombination mechanism.

At 77 K the diodes had a spectral cutoff of  $5.2 \mu\text{m}$ , quantum efficiency of 84 percent,  $R_0A$  product of  $2.3 \times 10^3 \Omega \cdot \text{cm}^2$ , and specific detectivity of  $1.7 \times 10^{11} \text{ cm} \cdot \text{Hz}^{1/2} \cdot \text{W}^{-1}$  at  $4.5 \mu\text{m}$  with  $84^\circ$  field of view and 300 K background, measured at zero bias with chopping frequency of 2.5 kHz. This result approaches the background-limited value for these conditions, which is  $2.4 \times 10^{11} \text{ cm} \cdot \text{Hz}^{1/2} \cdot \text{W}^{-1}$ . At reverse bias the detectivity is lower because of low-frequency noise having a  $1/f$  spectrum. The origin of this additional noise is not well understood at the present. It may be related to the origin of reverse current breakdown discussed in the next section, or to the contacts. The zero-bias detectivity at temperatures

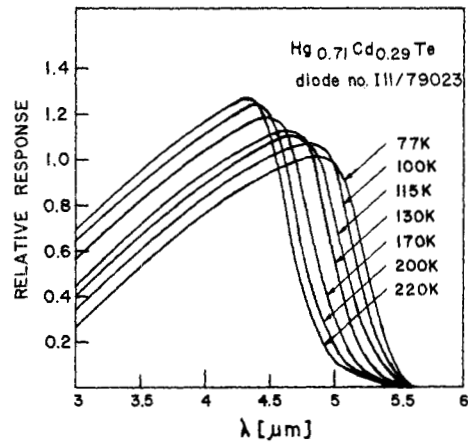


Fig. 4. Relative spectral response per watt of incident radiation at several operating temperatures. The cutoff wavelength decreases as the bandgap increases with temperature.

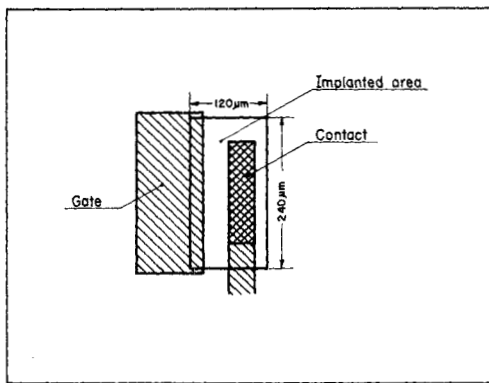


Fig. 5. Layout of the gate-controlled diode. The junction area is  $2.88 \times 10^{-4} \text{ cm}^2$ , total periphery is  $720 \times 10^{-4} \text{ cm}$ , and gate-controlled periphery is  $260 \times 10^{-4} \text{ cm}$ . The diode is covered by 5000 Å of ZnS. The implanted ion is boron,  $10^{15} \text{ cm}^{-2}$ , 150 keV.

higher than 160 K is limited by the diffusion current noise from the bulk.

It is interesting to note the dependence of cutoff wavelength on the operating temperature of the diode. We may define the experimentally observed cutoff as the wavelength at which responsivity falls to half its peak value and compare it to  $hc/E_G(T)$ , where  $E_G$  is given by (9). It comes out that the cutoff wavelengths expected from (9) are shorter than the experimental by 0.23-0.43 μm over the temperature range 77-200 K. This difference suggests that there may be a distinction between n-type and p-type material, since (9) was calculated from optical absorption in n-type material of the same composition.

V. GATE-CONTROLLED DIODES

We study next the reverse current using gate-controlled devices. It was found that an external electric field applied along the periphery of the junction has a major effect on the diode  $I-V$  characteristics. Gate-controlled diodes were made by using evaporated indium electrodes overlapping the edge of mesa diodes, insulated from the surface by a layer of ZnS or by native anodic oxide of HgCdTe [11], as shown in Fig. 5. The resulting three-terminal device characteristics

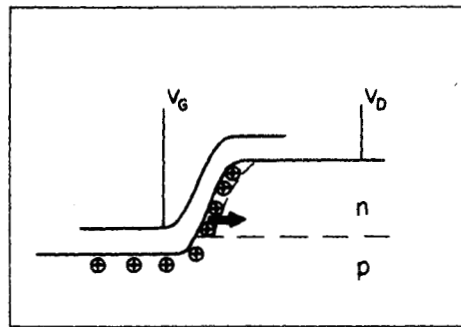
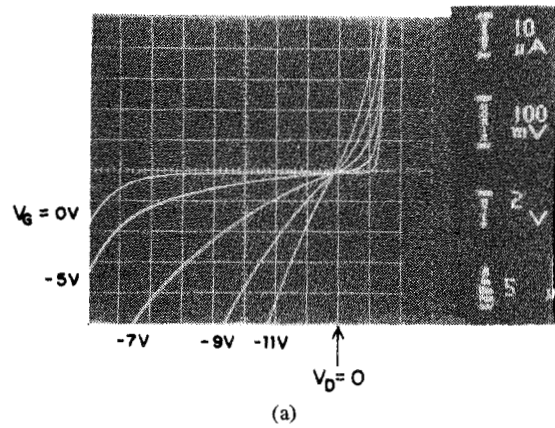


Fig. 6. (a) Current-voltage characteristics at 77 K for gate voltages below flat band (p-type side accumulated). (b) Schematic diagram showing the field-induced junction and tunneling current.

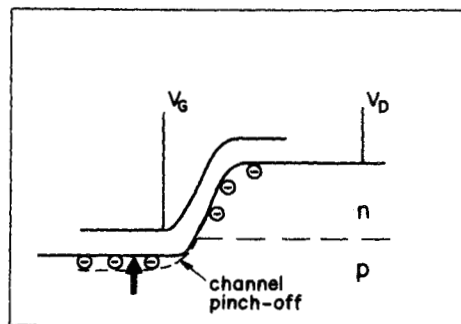
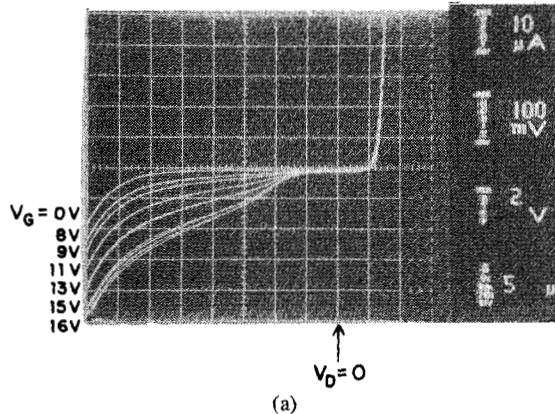


Fig. 7. (a) Current-voltage characteristics at 77 K for gate voltages above flat band (p-type side inverted). (b) Schematic diagram showing the field-induced junction, tunneling current, and channel pinchoff.

are shown in Figs. 6(a) and 7(a) with the gate voltage as a parameter.

In Fig. 6(a) the gate voltages are more negative than the flat-band voltage, causing surface accumulation in the p-type side and surface inversion in the implanted n-type side. The insulator in this device is ZnS, and the flat-band voltage, measured by independent  $C-V$  experiments, is +4.5 V, corresponding to an apparent negative interface charge  $Q_{ss}/q \approx 3 \times 10^{11} \text{ cm}^{-2}$ , typical for this interface [16]. The characteristics exhibit both reverse and forward tunneling currents. The forward injection current is high enough to mask the negative differential resistance in Fig. 6(a). Negative differential resistance was observed on some gate-controlled diodes with thin anodic oxide as gate insulator. Similar field-induced diode behavior has been observed in indium-antimonide for both diode polarities [17]. The device has been modeled by tunneling from the valence band of a field-induced inversion layer as shown in Fig. 6(b).

Fig. 7(a) shows the characteristics for gate voltages above flat band, forming an n-type surface inversion layer on the p side of the diode. It is seen that such gate voltages increase the leakage currents at reverse bias, and that there is a saturation value for the reverse current at each gate voltage. The same kind of characteristics, very similar to those of an MOS transistor, have been observed in silicon gate-controlled diodes [18], [19]. The saturation of reverse current indicates that carriers flow to the junction through an inversion channel, and that their flow is limited by channel pinchoff, as depicted in Fig. 7(b).

At high reverse bias the device is dominated by the sides of the junction which are not covered by a gate. Leakage current versus gate voltage for a fixed reverse junction bias exhibits a definite minimum near flat band. It should be noted that this minimum, which corresponds to the best diode characteristic, does not occur at zero-gate voltage, mainly due to the interface charge  $Q_{ss}$ . Tunneling currents start in field-induced junctions rather than the implanted junction, because the latter is linearly graded while the former may be regarded as true step junctions [19]. Thus the electric field intensity is always higher at the field-induced junction which is connected in parallel with the implanted junction.

Interband tunneling in HgCdTe has been treated theoretically by Anderson [20], as a physical limitation for the operation of charge injection devices in deep depletion. An exact quantitative comparison cannot be made between our results and the theory, since the active tunneling area is not known. However, the theory predicts a tunneling current density in the order of  $1 \text{ A} \cdot \text{cm}^{-2}$  for the doping level used in our samples and a band bending of 1 V, which is in reasonable agreement with our measurements, assuming that the width of the tunneling region is of the order of  $10 \mu\text{m}$ .

## VI. SUMMARY

Experimental results on ion-implanted n<sup>+</sup>-p photodiodes in  $\text{Hg}_{0.71}\text{Cd}_{0.29}\text{Te}$  have been presented. The n-type layer was found to be caused by implantation damage. Tunneling in this small-effective-mass narrow-gap material is a serious limitation for junction devices. We suggest that the tunneling

process takes place in field-induced junctions near the surface at the periphery of the implanted junction. Leakage current and differential resistance at zero bias may be dominated by the surface tunneling, unless the doping levels and surface potential are very well controlled. Photovoltaic detector performance of the implanted diodes has been evaluated as a function of temperature, exhibiting high quantum efficiency. Noise performance and  $R_0A$  product have been measured and calculated as a function of temperature. The maximum operating temperature was found to be limited by thermal diffusion noise, which may be reduced by an improvement of the minority-carrier lifetime in the substrate material.

## ACKNOWLEDGMENT

The authors wish to thank J. Shacham, S. Margalit, and T. Bernstein for their contributions to this work.

## REFERENCES

- [1] J. Marine and C. Motte, "Infrared photovoltaic detectors from ion-implanted  $\text{Cd}_x\text{Hg}_{1-x}\text{Te}$ ," *Appl. Phys. Lett.*, vol. 23, pp. 450-452, 1973.
- [2] P. J. McNally, "Development of (Hg, Cd)Te elevated temperature photovoltaic detectors," Interim Rep., Contract No. DAAK02-72-C-0331, Honeywell Radiation Center, 1973.
- [3] G. Fiorito, G. Gasparrini, and F. Svelto, "Advances in Hg implanted  $\text{Hg}_{1-x}\text{Cd}_x\text{Te}$  photovoltaic detectors," *I.R. Phys.*, vol. 15, pp. 287-293, 1975.
- [4] —, "Properties of Hg implanted  $\text{Hg}_{1-x}\text{Cd}_x\text{Te}$  infrared detectors," *Appl. Phys.*, vol. 17, pp. 105-110, 1978.
- [5] E. Igras, J. Piotrowski, and I. Z. Higersberger, "Investigation of ion-implanted graded gap (CdHg)Te photodiodes," *Electron Technol.*, vol. 10, pp. 63-69, 1977.
- [6] M. Lanir, A. H. B. Vanderwyck, and C. C. Wang, "Minority-carrier-lifetime determination in  $\text{Hg}_{0.68}\text{Cd}_{0.32}\text{Te}$ ," *J. Appl. Phys.*, vol. 49, pp. 6182-6184, 1978.
- [7] A. K. Sood and T. J. Tredwell, "High performance junction photodiodes for 8-14  $\mu\text{m}$  (Hg, Cd)Te infrared imaging applications," in *Proc. IEDM* (Washington, DC, 1978).
- [8] A. G. Foyt, T. C. Harman, and J. P. Donnelly, "Type conversion and n-p junction formation in  $\text{Hg}_{1-x}\text{Cd}_x\text{Te}$  produced by proton bombardment," *Appl. Phys. Lett.*, vol. 18, p. 321, 1971.
- [9] E. S. Johnson and J. L. Schmit, "Doping properties of selected impurities in  $\text{Hg}_{1-x}\text{Cd}_x\text{Te}$ ," *J. Electron. Mat.*, vol. 6, pp. 25-38, 1977.
- [10] C. Dearnaley, J. H. Freeman, R. S. Nelson, and J. Stephen, *Ion Implantation*. Amsterdam, The Netherlands: North-Holland, 1973, p. 766.
- [11] Y. Nemirovsky and I. Kidron, "The interface between  $\text{Hg}_{1-x}\text{Cd}_x\text{Te}$  and its native oxide," *Solid-State Electron.*, vol. 22, pp. 831-838, 1979.
- [12] S. Margalit, Y. Nemirovsky, and I. Rotstein, "Electrical properties of implanted  $\text{Hg}_{1-x}\text{Cd}_x\text{Te}$ ," to be published in *J. Appl. Phys.*
- [13] Y. Nemirovsky and E. Finkman, "Intrinsic carrier concentration of  $\text{Hg}_{1-x}\text{Cd}_x\text{Te}$ ," to be published in *J. Appl. Phys.*
- [14] C. T. Sah, R. N. Noyce, and W. Shockley, "Carrier generation and recombination in p-n junctions and p-n junction characteristics," *Proc. IRE*, vol. 45, pp. 1228-1243, 1957.
- [15] T. J. Tredwell, "Detection of long wavelength infrared at moderate temperatures," Final Tech. Rep., Apr. 1977, under NASA Contract NAS9-14180, N78-13876.
- [16] A. F. Tasch, R. A. Chapman, and B. H. Breazeale, "Field effect measurements on the HgCdTe surface," *J. Appl. Phys.*, vol. 41, pp. 4202-4204, 1970.
- [17] J. Shappir and S. Margalit, "Tunneling in field-induced diode in indium antimonide," *Solid-State Electron.*, vol. 19, pp. 789-794, 1976.
- [18] S. R. Hofstein and G. Warfield, "The insulated gate tunnel junction triode," *IEEE Trans. Electron Devices*, vol. ED-12, pp. 66-76, 1965.
- [19] A. S. Grove and D. J. Fitzgerald, "The origin of channel currents associated with  $p^+$  regions in silicon," *IEEE Trans. Electron*

- Devices*, vol. ED-12, pp. 619-626, 1965.
- [20] W. W. Anderson, "Tunnel current limitation of narrow bandgap infrared charge coupled devices," *I.R. Phys.*, vol. 17, pp. 147-164, 1977.
- [21] L. N. Swink and M. J. Brau, *Metallurgical Trans.*, vol. 1, p. 629, 1970.
- [22] R. A. Reynolds *et al.*, in *The Physics of Semimetals and Narrow-Gap Semiconductors*, D. L. Carter and R. T. Bate, Eds. New York: Pergamon, 1971, pp. 511-521.
- [23] I. M. Baker *et al.*, "Recombination in cadmium mercury telluride photodetectors," *Solid-State Electron.*, vol. 21, pp. 1475-1480, 1978.
- [24] J. L. Schmit, "Intrinsic carrier concentration of  $\text{Hg}_{1-x}\text{Cd}_x\text{Te}$  as a function of  $x$  and  $T$  using  $k \cdot p$  calculations," *J. Appl. Phys.*, vol. 41, pp. 2876-2879, 1970.
- [25] J. Shacham-Diamand, private communication.
- [26] D. L. Polla and A. K. Sood, "Schottky barrier photodiodes in  $\text{Hg}_{1-x}\text{Cd}_x\text{Te}$ ," in *Proc. IEDM* (Washington, DC, 1978).

## 1/f Noise in (Hg, Cd)Te Photodiodes

STEPHEN P. TOBIN, MEMBER, IEEE, SHIGESATO IWASA, AND TIMOTHY J. TREDWELL

**Abstract**—In this article we present results of experiments to characterize  $1/f$  noise in  $\text{Hg}_{0.7}\text{Cd}_{0.3}\text{Te}$   $n^+$ -on- $p$  junction photodiodes. Under zero-bias voltage conditions, the photodiodes display no  $1/f$  noise, even in the presence of large photocurrents. Under reverse-bias voltage operation,  $1/f$  noise is observed. In these experiments, the  $1/f$  noise was measured as a function of temperature, diode bias voltage, and photon flux. Since these parameters varied the relative contributions of the various current mechanisms, the diode current mechanism responsible for  $1/f$  noise was isolated. It was found that  $1/f$  noise is independent of photocurrent and diffusion current but is linearly related to surface generation current. It is proposed that  $1/f$  noise in reverse-biased (Hg, Cd)Te photodiodes is a result of modulation of the surface generation current by fluctuations in the surface potential.

### I. INTRODUCTION

EXCESS low-frequency noise, or  $1/f$  noise, has been an area of extensive investigation in a wide variety of semiconductor devices. Reduction of  $1/f$  noise is especially critical for infrared detectors due to the low frame rates at which many infrared imaging systems operate. The variable-bandgap semiconductor (Hg, Cd)Te has found wide applications as a photoconductor [1] for detection of 2-5- $\mu\text{m}$  and 8-14- $\mu\text{m}$  infrared radiation, due to its high electron mobility, long minority-carrier lifetime, and ease of preparation of low car-

rier concentration boules. Excess low-frequency noise in (Hg, Cd)Te photoconductors has been investigated by van der Ziel [2], who found a correlation between  $1/f$  noise and the presence of grain boundaries, and Broudy [3], who related  $1/f$  noise to surface potential variations and generation-recombination noise.

Recently, (Hg, Cd)Te photodiodes have been developed for both the 2-5- $\mu\text{m}$  [4], [5] and the 8-14- $\mu\text{m}$  [6] spectral regions. Because of the high impedance, low power dissipation, and linearity of photodiodes, high-density electronically scanned imaging arrays using (Hg, Cd)Te photodiodes are being developed [7]. However,  $1/f$  noise in HgCdTe photodiodes has not previously been investigated.

The current noise generated by a photodiode consists of a number of components, including shot noise due to photogenerated current, shot noise and thermal noise due to thermally generated (dark) current, and  $1/f$  noise. With the exception of  $1/f$  noise, the noise mechanisms are well understood [8] and are predictable from the device characteristics. The shot-noise current due to a photocurrent  $I_\phi$  is given by  $i_n^2 = 2qI_\phi$ . For a diode limited by diffusion current, the noise is the sum of the shot noise of the forward current  $I_D \exp(qV/kT)$  and the shot noise due to the reverse current  $-I_D$

$$i_n^2 = 2qI_D (\exp(qV/kT) + 1).$$

For depletion-layer generation-recombination current, the noise is the sum of the noise due to the generation current  $I_G(V)$  and the noise due to the recombination current  $I_R(V)$

$$i_n^2 = 2q(I_G(V) + I_R(V)).$$

The exact form of  $I_G$  and  $I_R$  depend, of course, on the junction profile, the trap energy, and cross sections. The measured

Manuscript received May 22, 1979; revised August 6, 1979. This work was partially supported by the Naval Electronic Systems Command, the Air Force Avionics Laboratory, and the Army Night Vision and Electro-Optics Laboratory under Naval Research Laboratory Contract N00173-77-C-0335.

S. P. Tobin and S. Iwasa are with Honeywell Electro-Optics Center, Lexington, MA 02173.

T. J. Tredwell was with Honeywell Electro-Optics Center, Lexington, MA. He is now with Eastman Kodak Research Laboratory, Rochester, NY.